Improving the Self-Guiding of an Ultraintense Laser by Tailoring Its Longitudinal Profile

M. Tzoufras,* F. S. Tsung, and W. B. Mori
Department of Physics and Astronomy, University of California, Los Angeles, California 90095, USA

A. A. Sahai
Department of Electrical and Computer Engineering, Duke University, Durham, North Carolina 27708, USA

(Received 27 July 2014; published 9 December 2014)

Self-guiding of an ultraintense laser requires the refractive index to build up rapidly to a sufficient value before the main body of the pulse passes by. We show that placing a low-intensity precursor in front of the main pulse mitigates the diffraction of its leading edge and facilitates reaching a self-guided state that remains stable for more than 10 Rayleigh lengths. Furthermore, this precursor slows the phase slippage between the trapped electrons and the wakefield and leads to an accelerating structure that is more stable, contains more energy, and is sustained longer. Examples from three-dimensional particle-in-cell simulations show that the conversion efficiency from the laser to the self-trapped electrons increases by an order of magnitude when using the precursor.

DOI: 10.1103/PhysRevLett.113.245001 PACS numbers: 52.38.Kd, 52.38.Hb, 52.65.Rr

Guiding of intense laser pulses is important for accelerating electrons in the laser wakefield accelerator concept as well as a fundamental topic in the area of nonlinear optics of plasmas. To achieve guided propagation of Gaussian laser beams in homogenous media the light itself must change the optical properties sufficiently to overcome diffraction. Such a modification can occur in rarefied plasmas, for pulses that quiver the plasma electrons with relativistic intensity, because the effective refractive index increases with the apparent electron mass γm_e. The necessary condition for relativistic self-focusing [1] is $P[\mathrm{GW}] > 17\omega_0^2/\omega_p^2 \equiv P_c$, where P and ω_0 are the laser power and frequency, and $\omega_p = \sqrt{4\pi e^2 n_e/m_e}$ is the plasma frequency. When $P > P_c$, the laser spot narrows until the ponderomotive force expels the plasma electrons and generates an ion channel [2]. Self-focusing is thus quenched at a "matched" spot, for which the restoring force from the ions to the electron sheath surrounding the channel cancels out the ponderomotive force.

In plasma-based acceleration an intense pulse of photons [3] or particles [4] creates a plasma wave wake. The electric field of this wake can be more than 3 orders of magnitude larger than in conventional accelerators; e.g., in Ref. [5] the energy of part of a 42 GeV electron beam doubled in less than 1 m. On the other hand, a powerful short laser pulse can drive the formation of a plasma bubble that facilitates the generation of quasimonoenergetic electron beams [6–11]. If this wakefield is sustained over centimeter to meter distances it can be used to generate electron beams with energies in excess of a GeV [12–16]. This requires that the laser travel stably through many Rayleigh lengths of underdense plasma, such that the accelerating structure (wakefield) is also stable.

Matching the laser spot size w_0 to the ion channel yields [11] $k_p R_b \sim k_p w_0 \sim \sqrt{a_0}$, where $a_0 = eA_0/(m_e c^2)$ is the normalized vector potential of the laser and $k_p R_b$ is the normalized channel radius with $k_p \equiv \omega_p/c$. The coefficients for this expression can be measured from 3D particle-in-cell (PIC) simulations, but the results differ depending on the laser and plasma conditions [11,17]. Furthermore, regardless of the initial spot size [18], and even if a plasma channel is used, the transverse laser envelope oscillates with a wavelength similar to the confocal parameter $b \equiv 2Z_R \equiv \omega_0 w_0^2/c$, suggesting that the balance of transverse forces alone does not ensure stable guiding.

For short pulses the ponderomotive force pushes plasma electrons forward as well as radially, raising the density ahead of the pulse and counteracting the effect of the relativistic mass on the refractive index $\eta = ck_0/\omega_0 = \sqrt{1-\omega_p^2/(\gamma\omega_0^2)}$. Therefore, part of the pulse (approximately c/ω_p) is lost every Rayleigh length even if $P > P_c$, hindering self-guiding for single-frequency pulses [19] with duration $\tau_L \lesssim 2\pi/\omega_p$. Preformed density channels [20] may then be used to prevent the head of the laser from diffracting.

Simulations have nevertheless demonstrated that ultraintense short lasers propagate stably in homogenous plasmas after some initial stages of evolution. Early in the interaction the laser energy within the spot size at the front of the pulse is lost due to diffraction and localized pump depletion. The leading edge of the pulse falls backwards while the rest stays guided [21]. In transferring energy to the plasma, the leading photons slow down causing the front of the pulse to redshift and generating a positive frequency chirp [22]. The steepening of the pulse

front, together with the diffraction of the leading edge, eventually produces an optical shock [23]. The front of the shock then etches backwards [21] at a rate $v_{\rm etch} \simeq c\omega_p^2/\omega_0^2$. The formation and propagation of such shocklike pulse shapes may be described as a two-stage process [24]: first the pulse self-steepens, then its leading edge etches back. The first stage is associated with diffraction of the pulse front and oscillations of the laser envelope and can be extended by introducing a negative frequency chirp [25,26]. But the second stage is more stable and more efficient at converting the laser energy to usable energy in the wakefield.

The first stage can be shortened and the losses due to diffraction can be reduced by increasing the plasma density, because the distance for the optical shock to form scales as $L_{s1} \propto (k_0/k_p)(1/a_0^2)Z_R$. This is the distance for the frequency chirp to form and to derive it we assume a matched transverse spot size and substitute into Eq. (2.21) in Ref. [24]. However, high plasma density limits the overall acceleration distance [11], and it precipitates laser-plasma instabilities that bring about the filamentation [27] and hosing [28–31] of laser light and the associated generation of postsoliton structures [32,33].

To mitigate diffraction and guide the laser at lower densities, we propose adding a precursor that—like the bulbous bow of ocean liners—drives a suitable response from the medium to enable the propagation of the main body of the pulse. The low-intensity precursor is introduced to raise the refractive index by adiabatically pushing the plasma electrons transversely. It is needed while the main pulse is evolving to a shocklike profile. Afterwards, the shocklike pulse will remain focused, even as the precursor gradually diffracts away. The peak precursor power approaches P_c and its rise time is long enough to minimize the longitudinal ponderomotive force. Unlike radius-tailored pulses, proposed in Ref. [34], we are proposing a precursor with the spot size equal to that of the main pulse, and we are considering very intense main pulses. After the shocklike profile has been reached, a fraction of the leading edge depletes before it can diffract. The balance between diffraction and pump depletion can be studied with PIC simulations.

To explore the effect of this longitudinal profile on laser guiding and electron acceleration, we performed 3D PIC simulations with the code OSIRIS [35]. We set the ratio $\omega_p^2/\omega_0^2 = 8.4 \times 10^{-4}$, which for a laser with $\lambda_0 = 0.8$ μm yields $n_e = 1.47 \times 10^{18}$ cm^{-3}. The simulation domain is $1200c/\omega_0 \times 2000c/\omega_0 \times 2000c/\omega_0$ and it moves in the direction of the laser propagation with the speed of light. A $6000 \times 512 \times 512$ mesh with two particles per cell and absorbing transverse boundaries [36] is used. A reference simulation was performed for a linearly polarized pulse with spot size $w_0 = 9.7$ μm, maximum power $P = 200$ TW $\simeq 10P_c$, $a_0 = 8$, rise time [37] $\tau_r = 4.2$ fs and fall time $\tau_f = 86$ fs, with total energy 7.8 J and an effective $\tau_{\rm FWHM} \simeq 33$ fs. In a second simulation, a precursor was added as shown in Fig. 1(a) with $P_p = 20$ TW $\simeq P_c$, $a_{0,p} = 2.5$, rise time $\tau_{r,p} = 212$ fs, $\tau_{f,p} = 4.2$ fs, and energy 1.7 J. Two-dimensional half slices of the initial laser electric field with and without the precursor are shown in Figs. 1(b) and 1(c).

In Figs. 1(d)–1(e) we show the normalized laser electric field after 0.71 cm, where $Z_R = 0.037$ cm for the initial spot size. The amplitude of the reference pulse is about half that of the tailored pulse. Because of the initial energy loss, the reference pulse no longer generates a plasma bubble after 0.71 cm and its wake is unsuitable for accelerating electrons. On the contrary, the tailored pulse has formed an optical shock and remains guided for the rest of the simulation. A symmetric Gaussian pulse behaves similarly as the reference case; e.g., in Ref. [11] a symmetric pulse with the same energy and power as the reference pulse, and spot size more than 2 times wider, accelerated electrons up to 0.75 cm before depleting.

The wake structure is shown in Figs. 2(a) and 2(b) from the reference case and in Figs. 2(c) and 2(d) from the precursor case. For both cases the plasma bubble is initially [Figs. 2(a) and 2(c)] excited at about the same location with similar wakefield E_x in the accelerating region [lineouts along the propagation axis in Fig. 2(e)]. The transverse ponderomotive force of the precursor produces an electron density channel with small and relatively

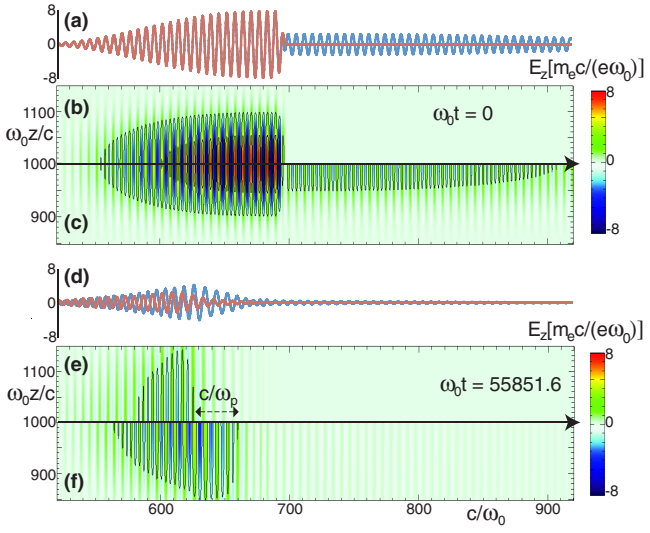

FIG. 1 (color online). 3D PIC simulations demonstrate that a pulse with sharp rise time diffracts while a pulse with tailored profile remains guided. (a) The laser electric field $E_z(x, t = 0)$ for a pulse with sharp rise time (red) and for the precursor of a tailored pulse (blue); the main bodies of the two pulses are identical. The top half of a 2D slice of $E_z(x, y, t = 0)$ for a pulse with sharp rise time is shown in (b) and the bottom half of a slice of $E_z(x, y, t = 0)$ for a tailored pulse in (c). Contours have been drawn for $(e\omega_0 E_z/m_e c) = \pm 1.6, \pm 4.8$. Plots (d), (e), and (f) correspond to (a), (b), and (c) at $\omega_0 t = 55\,951.6$.

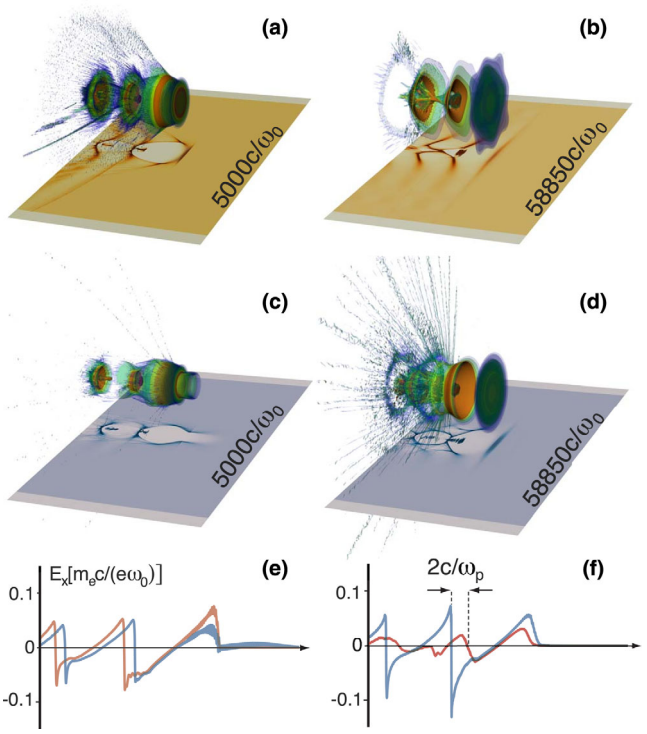

FIG. 2 (color online). Electron density isosurfaces and slices from two 3D PIC simulations, the same as in Fig. 1. In (a) and (b) a pulse with sharp rise time [Fig. 1(b)] is used. In (c) and (d) the pulse has a tailored profile [Fig. 1(c)]. Panels (e) and (f) show the electric field $E_x(x)$ along the laser propagation axis with red (blue) lines for the sharp (tailored) profile.

constant decelerating field, and a corresponding refractive index that leads to redshifting of the laser. This is analogous to the effect of an adiabatically ramped electron beam driver in plasma wakefield accelerators [38,39]. The early dynamics and phase space of the trapped electrons are almost identical in these two simulations. No oscillations of the laser envelope are observed; instead, because the initial spot size is too narrow, both pulses defocus slightly. Subsequently, the tailored pulse stabilizes at a wider spot, even as the reference pulse continues to slowly defocus.

After approximately $10Z_R$ the reference pulse is nearly exhausted and cannot stay guided. As it diffracts it drives the weak response shown in Fig. 2(b) after $\sim 20Z_R$. Its wake does not contain enough energy to support the trapped electrons and most of them decelerate due to excessive beam loading [40,41]. In contrast, the wake of the tailored pulse has retained a significant amount of energy. Moreover, the leading edge of the tailored pulse has receded less [Fig. 1(f) versus Fig. 1(e)], preventing the trapped electrons from slipping forward with respect to the wake, and allowing them to spend more time at the rear of the bubble, where the accelerating force is larger. Figure 2(d) shows that the accelerating structure generated by the tailored pulse is stable and electrons continue to get injected and accelerated. Its wake extends $2c/\omega_p$ behind the reference even though its leading edge is c/ω_p ahead. Therefore, much more energy is available behind the tailored pulse while a lot of energy still remains in its fields.

The increase in the acceleration distance is also seen from Fig. 3, where the maximum decelerating field [Fig. 3(a)] and the amplitude of the laser electric field [Fig. 3(b)] are plotted in terms of the propagation distance. The sensitivity on the initial laser spot size was examined with a third 3D simulation, where w_0 was raised by 50% throughout the pulse and the intensity was reduced accordingly to maintain the same power profile as that for the tailored pulse with $a_0 = 8$. After focusing to a narrow spot, the tailored pulse with $a_0 = 5.3$ exhibits the same behavior as that for $a_0 = 8$.

The simulations with tailored pulses enter the optical shock stage at around $1/3$ of the total propagation distance (1.65 cm), and at that point the injection of electrons into the plasma bubble becomes continuous. As the number of trapped electrons keeps increasing, and the laser keeps depleting, their charge eventually becomes high enough to prevent the blown-out plasma electrons from returning on axis [10]. After 1.65 cm the peak energy is reached and the laser energy is completely exhausted. The wake created by the injected beam exceeds that from the depleted laser and the front group of electrons begins to lose energy. The acceleration distance reaches 1.65 cm, more than $40Z_R$ for the initial spot size, and more than 2 times longer than in the reference simulation with only 20% more laser energy.

The ultimate goal in the laser wakefield accelerator is to couple controlled injection in a short section with acceleration in a long section. For simplicity, we have not modeled a separate injection section. Although the self-injected electron bunches in our simulations are not of high quality, the total energy in the output beams and their spectra further illustrate how the precursor improves the efficiency

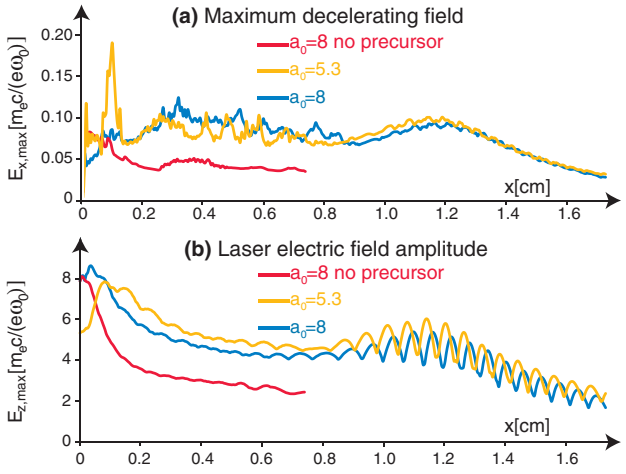

FIG. 3 (color online). (a) The maximum decelerating field (which scales with the accelerating field) and (b) the amplitude of the laser electric field, shown in terms of the propagation distance from three simulations: without a precursor for $a_0 = 8$, and with a precursor for $a_0 = 8$ and $a_0 = 5.3$.

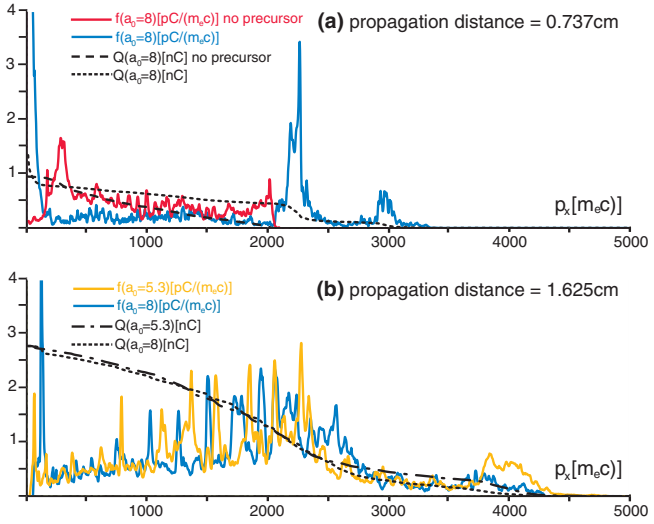

FIG. 4 (color online). (a) Energy distributions after 0.737 cm shown from a simulation of a pulse with (without) a precursor blue (red). The energy of particles above 100 MeV is ~0.73 J and ~0.43 J, respectively. The charge $Q(p_x) = \int_{p_x}^{\infty} f(p'_x)dp'_x$ is shown with broken or dotted lines. (b) Two spectra after 1.625 cm for two tailored pulses with different initial w_0, a_0 but the same power profile. The blue and dotted lines are from the same simulation as in (a). The energy in electrons above 100 MeV (1 GeV) is 2.74 J (1.9 J) for the simulation with $a_0 = 5.3$ and 2.61 J (1.86 J) for the simulation with $a_0 = 8$.

of the process. In Fig. 4(a) we compare the spectra from the two simulations with $a_0 = 8$ after 0.737 cm. The broken or dotted lines show $Q(p_x) = \int_{p_x}^{\infty} f(p'_x)dp'_x$. The total charge is similar for these two cases, but the spectra are very different. For the simulation with the tailored profile the maximum energy corresponds to $p_x \gtrsim 3000 m_e c$ (i.e., $E \gtrsim 1.5$ GeV), and there is 0.73 J of energy in electrons above 100 MeV. For the reference simulation the corresponding numbers are $2000 m_e c$ and 0.43 J.

In Fig. 4(b) the distribution from the simulation with the tailored pulse is also shown after 1.625 cm. The maximum p_x exceeds $4200 m_e c$ ($E \gtrsim 2.15$ GeV) and the energy in particles above 100 MeV is 2.61 J. Hence, 27.5% of the laser energy (including the precursor) is converted to electrons above 100 MeV. Most of the energy transfer takes place after 0.737 cm [Fig. 4(a)], when the self-injection is continuous and the wake is heavily loaded. During the early stage of acceleration, the energy transfer from the laser to the trapped electrons is not very effective, because the pulse is still evolving to the optical shock profile, and because there are not enough trapped electrons to ensure high beam loading efficiency. At 1.625 cm the distribution comprises two populations of electrons. Electrons injected during the first stage of pulse evolution have relatively high energy and reside at the head of the accelerating bunch. Those trapped during the continuous injection stage have a continuous energy spectrum extending to 2.15 GeV, higher than what is achieved in the reference case (1 GeV) or what is possible with a similar symmetric pulse (1.5 GeV in Ref. [11]).

With $a_0 = 5.3$ the peak energy is again reached after 1.625 cm and the energy distribution is shown in Fig. 4(b). Electrons trapped early in the third simulation reach slightly higher energy compared to those in the second, and this is manifested as an increase in the number of electrons at ~2 GeV in Fig. 4(b). Aside from that, the spectra for the tailored profiles with $a_0 = 5.3$ and $a_0 = 8$ are similar.

For pulses with symmetric Gaussian profiles, envelope oscillations can generate quasimonoenergetic electron bunches, because faster pulse depletion curtails the stage of continuous injection. However, the peak electron energy is not as high as that produced for the tailored pulses proposed here. More importantly, when using a tailored profile the efficiency is an order of magnitude higher, with nearly 30% of the laser energy converted to accelerated electrons. Even higher efficiency, as well as narrow energy spread [24], can be achieved by externally injecting the plasma bubble with electrons to optimize beam loading.

Two-dimensional simulations indicate that these improvements are weakly sensitive to the details of the longitudinal profile. As long as the precursor can increase the refractive index without driving a large longitudinal electric field, and as long as the main body of the pulse rises sharply and high enough to generate a plasma bubble in its wake, both the peak energy and the efficiency will be enhanced compared to symmetric pulses.

We acknowledge useful discussions with Dr. J. Vieira and Ms. J. Shaw. Simulations were performed on the Hoffman2 cluster at UCLA, on the Blue Waters supercomputer at the National Center for Supercomputing Applications, and on the Chanakya cluster at Duke University. Work was supported by the U.S. Department of Energy under Grants No. DE-SC-0008491, No. DE-SC-0008316, No. DE-FG02-92ER40727, No. DE-NA-0001833, and No. DE-SC0010012, and by the U.S. National Science Foundation under Grants No. ACI-1339893, No. OCI-1036224, and No. NSF-PHY-0936278.

*mtzoufras@physics.ucla.edu

[1] P. Sprangle, C.-M. Tang, and E. Esarey, IEEE Trans. Plasma Sci. **15**, 145 (1987).
[2] G.-Z. Sun, E. Ott, Y. C. Lee, and P. Guzdar, Phys. Fluids **30**, 526 (1987).
[3] T. Tajima and J. M. Dawson, Phys. Rev. Lett. **43**, 267 (1979).
[4] P. Chen, J. M. Dawson, R. W. Huff, and T. Katsouleas, Phys. Rev. Lett. **54**, 693 (1985).
[5] I. Blumenfeld, C. E. Clayton, F.-J. Decker, M. J. Hogan, C. Huang, R. Ischebeck, R. Iverson, C. Joshi, T. Katsouleas, N. Kirby, W. Lu, K. A. Marsh, W. B. Mori, P. Muggli, E. Oz, R. H. Siemann, D. Walz, and M. Zhou, Nature (London) **445**, 741 (2007).

[6] A. Pukhov and J. Meyer-ter Vehn, Appl. Phys. B **74**, 355 (2002).

[7] S. P. D. Mangles, C. D. Murphy, Z. Najmudin, A. G. R. Thomas, J. L. Collier, A. E. Dangor, E. J. Divall, P. S. Foster, J. G. Gallacher, C. J. Hooker, D. A. Jaroszynski, A. J. Langley, W. B. Mori, P. A. Norreys, F. S. Tsung, R. Viskup, B. R. Walton, and K. Krushelnick, Nature (London) **431**, 535 (2004).

[8] C. G. R. Geddes, Cs. Toth, J. van Tilborg, E. Esarey, C. B. Schroeder, D. Bruhwiler, C. Nieter, J. Cary, and W. P. Leemans, Nature (London) **431**, 538 (2004).

[9] J. Faure, Y. Glinec, A. Pukhov, S. Kiselev, S. Gordienko, E. Lefebvre, J. P. Rousseau, F. Burgy, and V. Malka, Nature (London) **431**, 541 (2004).

[10] F. S. Tsung, R. Narang, W. B. Mori, C. Joshi, R. A. Fonseca, and L. O. Silva, Phys. Rev. Lett. **93**, 185002 (2004).

[11] W. Lu, M. Tzoufras, C. Joshi, F. S. Tsung, W. B. Mori, J. Vieira, R. A. Fonseca, and L. O. Silva, Phys. Rev. ST Accel. Beams **10**, 061301 (2007).

[12] W. P. Leemans, B. Nagler, A. J. Gonsalves, Cs. Toth, K. Nakamura, C. G. R. Geddes, E. Esarey, C. B. Schroeder, and S. M. Hooker, Nat. Phys. **2**, 696 (2006).

[13] S. Kneip, S. R. Nagel, S. F. Martins, S. P. D. Mangles, C. Bellei, O. Chekhlov, R. J. Clarke, N. Delerue, E. J. Divall, G. Doucas, K. Ertel, F. Fiuza, R. Fonseca, P. Foster, S. J. Hawkes, C. J. Hooker, K. Krushelnick, W. B. Mori, C. A. J. Palmer, K. Ta Phuoc *et al.*, Phys. Rev. Lett. **103**, 035002 (2009).

[14] C. E. Clayton, J. E. Ralph, F. Albert, R. A. Fonseca, S. H. Glenzer, C. Joshi, W. Lu, K. A. Marsh, S. F. Martins, W. B. Mori, A. Pak, F. S. Tsung, B. B. Pollock, J. S. Ross, L. O. Silva, and D. H. Froula, Phys. Rev. Lett. **105**, 105003 (2010).

[15] P. A. Walker, N. Bourgeois, W. Rittershofer, J. Cowley, N. Kajumba, A. R. Maier, J. Wenz, C. M. Werle, S. Karsch, F. Grüner, D. R. Symes, P. P. Rajeev, S. J. Hawkes, O. Chekhlov, C. J. Hooker, B. Parry, Y. Tang, and S. M. Hooker, New J. Phys. **15**, 045024 (2013).

[16] S. F. Martins, R. A. Fonseca, W. Lu, W. B. Mori, and L. O. Silva, Nat. Phys. **6**, 311 (2010).

[17] S. Gordienko and A. Pukhov, Phys. Plasmas **12**, 043109 (2005).

[18] M. Tzoufras, Ph.D. thesis, UCLA, 2008.

[19] P. Sprangle, E. Esarey, and A. Ting, Phys. Rev. Lett. **64**, 2011 (1990).

[20] W. P. Leemans, C. W. Siders, E. Esarey, N. E. Andreev, G. Shvets, and W. B. Mori, IEEE Trans. Plasma Sci. **24**, 331 (1996).

[21] C. D. Decker, W. B. Mori, K.-C. Tzeng, and T. Katsouleas, Phys. Plasmas **3**, 2047 (1996).

[22] W. B. Mori, IEEE J. Quantum Electron. **33**, 1942 (1997).

[23] J. Vieira, F. Fiúza, L. O. Silva, M. Tzoufras, and W. B. Mori, New J. Phys. **12**, 045025 (2010).

[24] M. Tzoufras, C. Huang, J. H. Cooley, F. S. Tsung, J. Vieira, and W. B. Mori, J. Plasma Phys. **78**, 401 (2012).

[25] S. Y. Kalmykov, A. Beck, X. Davoine, E. Lefebvre, and B. A. Shadwick, New J. Phys. **14**, 033025 (2012).

[26] V. B. Pathak, J. Vieira, R. A. Fonseca, and L. O. Silva, New J. Phys. **14**, 023057 (2012).

[27] P. Kaw, G. Schmidt, and T. Wilcox, Phys. Fluids **16**, 1522 (1973).

[28] P. Sprangle, J. Krall, and E. Esarey, Phys. Rev. Lett. **73**, 3544 (1994).

[29] G. Shvets and J. S. Wurtele, Phys. Rev. Lett. **73**, 3540 (1994).

[30] B. J. Duda, R. G. Hemker, K. C. Tzeng, and W. B. Mori, Phys. Rev. Lett. **83**, 1978 (1999).

[31] B. J. Duda and W. B. Mori, Phys. Rev. E **61**, 1925 (2000).

[32] N. M. Naumova, S. V. Bulanov, T. Z. Esirkepov, D. Farina, K. Nishihara, F. Pegoraro, H. Ruhl, and A. S. Sakharov, Phys. Rev. Lett. **87**, 185004 (2001).

[33] G. Sarri, D. K. Singh, J. R. Davies, F. Fiuza, K. L. Lancaster, E. L. Clark, S. Hassan, J. Jiang, N. Kageiwa, N. Lopes, A. Rehman, C. Russo, R. H. H. Scott, T. Tanimoto, Z. Najmudin, K. A. Tanaka, M. Tatarakis, M. Borghesi, and P. A. Norreys, Phys. Rev. Lett. **105**, 175007 (2010).

[34] J. Krall, E. Esarey, P. Sprangle, and G. Joyce, Phys. Plasmas **1**, 1738 (1994).

[35] R. A. Fonseca, L. O. Silva, F. S. Tsung, V. K. Decyk, W. Lu, C. Ren, W. B. Mori, S. Deng, S. Lee, T. Katsouleas, and J. C. Adam, in *Computational Science - ICCS 2002, International Conference, Amsterdam, The Netherlands, April 21-24, 2002. Proceedings, Part III*, Lecture Notes in Computer Science Vol. 2331, edited by P. M. A. Sloot, C. Jeng Kenneth Tan, J. Dongarra, and A. G. Hoekstra, (Springer, New York, 2002), pp. 342–351.

[36] J.-L. Vay, J. Comput. Phys. **165**, 511 (2000).

[37] A polynomial temporal profile is used for the laser pulse $a(\tau)/a_0 = 10\tau^3 - 15\tau^4 + 6\tau^5$, where $0 \le \tau \le 1$ with τ normalized to the rise time or fall time, to mimic a Gaussian profile with $e^{-(1-\tau)^2/0.625^2}$.

[38] K. L. F. Bane, P. Chen, and P. B. Wilson, IEEE Trans. Nucl. Sci., **32**, 3524 (1985).

[39] P. Chen, A. Spitkovsky, T. Katsouleas, and W. B. Mori, Nucl. Instrum. Methods Phys. Res., Sect. A **410**, 488 (1998).

[40] M. Tzoufras, W. Lu, F. S. Tsung, C. Huang, W. B. Mori, T. Katsouleas, J. Vieira, R. A. Fonseca, and L. O. Silva, Phys. Rev. Lett. **101**, 145002 (2008).

[41] M. Tzoufras, W. Lu, F. S. Tsung, C. Huang, W. B. Mori, T. Katsouleas, J. Vieira, R. A. Fonseca, and L. O. Silva, Phys. Plasmas **16**, 056705 (2009).